Available online at www.sciencedirect.com
ScienceDirect
Journal of Colloid and Interface Science 304 (2006) 524–529
Journal of Colloid and Interface Science
www.elsevier.com/locate/jcis

Adhesion as an interplay between particle size and surface roughness

J. Katainen [a,*], M. Paajanen [a], E. Ahtola [a], V. Pore [b], J. Lahtinen [a]

[a] Laboratory of Physics, Helsinki University of Technology, P.O. Box 1100, FI-02015 TKK, Finland
[b] Department of Chemistry, P.O. Box 55, University of Helsinki, FI-00014, Finland

Received 30 May 2006; accepted 9 September 2006

Available online 14 September 2006

Abstract

Surface roughness plays an important role in the adhesion of small particles. In this paper we have investigated adhesion as a geometrical effect taking into account both the particle size and the size of the surface features. Adhesion is studied using blunt model particles on surfaces up to 10 nm root-mean-square (RMS) roughness. Measurements with particles both smaller and larger than surface features are presented. Results indicate different behavior in these areas. Adhesion of particles smaller than or similar in size to the asperities depend mainly on the size and shape of the asperities and only weakly on the size of the particle. For large particles also the particle size has a significant effect on the adhesion. A new model, which takes the relative size of particles and asperities into account, is also derived and compared to the experimental data. The proposed model predicts adhesion well over a wide range of particle/asperity length scales.
© 2006 Elsevier Inc. All rights reserved.

Keywords: Adhesion; Surface roughness; Pull-off force; Atomic force microscope

1. Introduction

Hardly any real surface is smooth at a submicroscopic level. Practical surfaces often possess significant roughness and even highly polished silicon wafers in semiconductor industry are rough in subnanometer scale [1]. Surface roughness plays an important role in adhesion since it reduces the contact area between the bodies leading to significantly reduced interaction [2–4]. Surfaces may posses roughness in several length scales, but due to the short range of the van der Waals interaction, roughness in nanoscale ultimately determines the strength of adhesion.

Invention and progress of colloidal probe technique have boosted the studies of adhesion and the effects of nanoscale roughness [5]. In order to explain experimentally observed adhesion on rough surfaces, both analytical [6–8] and computational [9–11] approaches have been used. While computational methods produce good agreement with experiments [11,12], they are complex and thus not easily applied for fast estimation of the adhesion for specific systems. On the other hand, analytical equations rely on only few parameters which are easily determined from the surface topography. This ensures that they can be easily used for multiple systems to estimate the adhesion [13,14].

Recent models are based on approach where the asperities are assumed to be hemispherical caps on a smooth substrate [6]. Rabinovich et al. [7,8] have suggested that the adhesion on surfaces exhibiting asperities should be written as a combination of sphere–sphere and sphere–surface interactions in the form

$$F_{\mathrm{adh}} = \frac{\mathcal{A}_{\mathrm{H}} R}{6 H_0^2}\left[\frac{r}{r+R} + \frac{1}{(1+y_{\max}/H_0)^2}\right], \tag{1}$$

where $\mathcal{A}_{\mathrm{H}}$ is the Hamaker constant, R is the radius of the adhering particle, H_0 is the equilibrium distance, r is the radius of the asperity on the surface, and $y_{\max}$ is the height of the asperity. The first term is the adhesion between the asperity and the particle, separated by H_0 and the second term the contribution of the particle–substrate interaction. Fig. 5a illustrates the contact geometry used in deriving Eq. (1). This approach overestimates the adhesion because the last term takes the whole interacting surface into account as a plane, resulting in double counting of the contribution of the substrate under the asperity. To reduce the effect of double counting, a condition $R \gg r$ must apply in-

* Corresponding author. Fax: +358 9 451 3116.
E-mail address: jukka.katainen@tkk.fi (J. Katainen).

0021-9797/$ – see front matter © 2006 Elsevier Inc. All rights reserved.
doi:10.1016/j.jcis.2006.09.015

dicating that the adhering particle is much larger than a single asperity.

When the particle and the substrate are of different materials, the Hamaker constant can be calculated from

$$\mathcal{A}_{H_{12}} = \sqrt{\mathcal{A}_{H_{11}}\mathcal{A}_{H_{22}}}. \quad (2)$$

In this work we have demonstrated that although the model by Rabinovich et al. gives reasonable estimates for pull-off forces with particles comparable in size with the asperities on the surface, it underestimates the adhesion if the particles are much larger than the asperities. We have derived a new model for this region which takes into account multiple contacts with the surface. The new model has been tested by comparison to experimental data over a wide range of particle/asperity sizes. The comparison illustrated that both models are needed to cover the whole experimental range.

2. Experimental methods

2.1. Surfaces

Polycrystalline TiO_2 thin films prepared by atomic layer deposition (ALD) were used as the studied surfaces. ALD is a gas phase thin film deposition method which produces uniform and high quality thin films with good reproducibility [15]. The films were grown on borosilicate glass substrates using a process described earlier [16]. The deposition temperature was 620 K resulting in anatase structure. Films with three different surface geometries were prepared by varying the film thickness.

Table 1
Properties of the rough TiO_2 films. Radius of curvature and height represent properties of the typical asperity on the surface

Film thickness (nm)	Rms roughness (nm)	Density of asperities ρ ($1/\mu m^2$)	Radius of curvature r (nm)	Height y_{max} (nm)
10	0.65	880	30 ± 13	1.5 ± 0.5
130	6.2	270	10 ± 2	15 ± 4
500	11	120	13 ± 2	26 ± 9

The surfaces were imaged using a Digital Instruments Nanoscope III with extender electronics. The main properties of the films are presented in Table 1. The density of asperities is determined from the number of grains on the 1 μm^2 topographic AFM images. The local maxima were identified from the images, and maxima that do not exceed a preset height level were excluded. The limit was determined using the height distribution of the surface and set half width at half maximum (HWHM) above the mean surface level. A paraboloid was fitted to each accepted local maxima. Each paraboloid was allowed to find an optimal shape and location. The radii of curvature at the apexes of the fitted paraboloids were used as the radii of the asperities. The heights of the grains were determined as the difference between the apex of the fitted parabola and an estimated value for the surface level around the grain. The surface level was calculated individually for each asperity. Distributions of radii of curvatures and heights are presented in Fig. 1 for all three surfaces used in the experiments. Since the acceptance limit for asperities is chosen arbitrarily, the number of grains is more indicative than absolute. In addition to these accepted maxima there were also a number of low local maxima, which we expect not to contribute to the adhesion. Also, it should be noted that the asperity curvature of the two roughest surfaces is very close to the standard AFM tip apex curvature, indicating very sharp asperities. This is due to the crystallinity of the coatings.

2.2. Particles

Eroded silicon tips exhibiting flat apexes with native oxide were used as blunt silica particles. The flat apex of different size were made by eroding fresh tips against a silicon sample. Approximate scanning parameters during erosion were: scan size 4 μm, rate 4 Hz, normal force 50 nN, and angles 0°, 45°, 90°, and 135°. The apex size was controlled by the erosion time, though also some variations on the normal force were used. Single crystal silicon cantilevers were calibrated by the Sader et al. method [17] by the manufacturer (CSC17-F, Mikro-

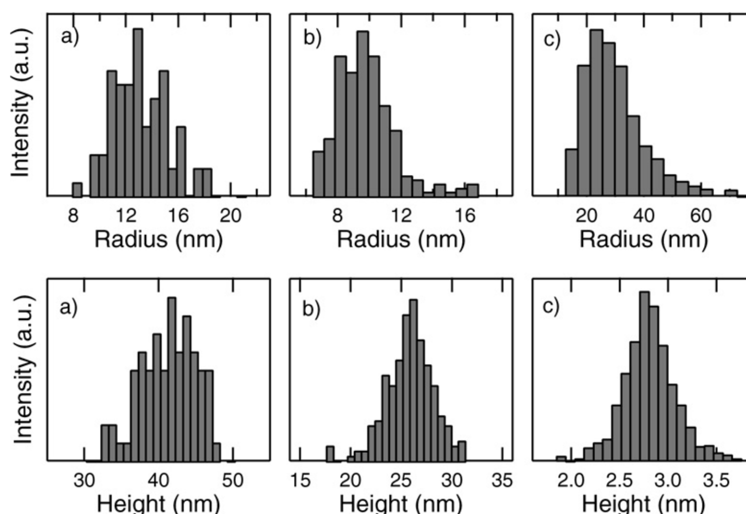

Fig. 1. Radius (top) and height (bottom) distributions of the asperities on the samples. (a) 500-, (b) 130-, and (c) 10-nm thick TiO_2 coating on borosilicate glass.

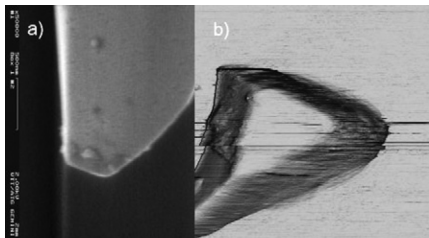

Fig. 2. One of the tips used imaged by (a) SEM and (b) reverse AFM. The AFM image is obtained by scanning the tip over a sample with an array of sharp peaks. The color scale in the AFM image represents gradient on the surface.

masch, Spain). The spring constants varied between 0.13 and 0.23 N/m.

Reverse AFM imaging in contact mode was used to image the blunt particles: The probe of interest was used in imaging a silicon reference grating with an array of sharp needles (TGT01, Mikromasch). Since the probes were significantly larger than the needles on the surface, the resulted image represents the topography of the probe instead of the grating.

Total of eight different AFM tips were used as particles. One of the eroded tips is shown in Fig. 2 with the flat apex clearly visible. The areas of the flax apexes of the tips determined from the AFM images varied between 600 ± 200 and $47{,}000 \pm 7000$ nm^2. However, it should be noted that the smaller the tip the rounder it is, thus the values for smallest tips are more like effective areas than the real areas of flat apexes.

2.3. Pull-off force measurements

The measurements reported here were also performed using the Nanoscope III. The measurements were done under an atmospheric hood in ambient temperature and pressure. The humidity was kept under RH 5% during the measurements by flowing dry nitrogen (99.5%, AGA, Finland) through the hood. The relative humidity and temperature were continuously monitored with Vaisala HMP233 humidity meter (accuracy better than RH $\pm 1\%$).

The pull-off forces were measured as displacement–deflection curves by moving the sample and measuring the cantilever deflection as a function of the sample position. The loading was kept under 10 nN and constant during measurements although no effect of the load on the pull-off force was detected when tested. Ramp sizes from 100 to 3000 nm were used for different probe–surface pairs. The speed of the probe was kept at constant value of 1500 nm/s by varying the scan rate according to the ramp size. In order to guarantee sufficient statistics on rough surfaces, displacement–deflection curves were recorded in 20×20 matrix with lateral step of 100 nm. In addition, such matrix was measured repeatedly in 6 locations on the surface. The measurements thus resulted to 2400 single displacement–deflection curves for each probe–surface pair covering 24 μm^2 of the surface. After each set of measurements the probe was gently scanned on a silicon surface to ensure the removal of possible contamination. The probe was then stored for at least 12 h before the next measurement to allow native oxidation of the possibly exposed silicon. The same process was also performed if the pull-off force decreased dramatically during a measurement, most likely due to particle contamination.

The pull-off forces were automatically extracted from the displacement–deflection curves. The zero deflection was set to an average value of the retracting curve after the pull-off. Lines were fitted to the contact part and the vertical pull-off part and the intersection of these lines with the zero deflection were used to calculate the distance the Z-piezo traveled before the pull-off. This distance equals to the deflection of the cantilever at the pull-off and was converted to pull-off force by multiplying with the force constant of the cantilever. Using the Z movement of the piezo tube to directly obtain the pull-off force avoids the nonlinear conversion of the photodiode voltage to cantilever deflection. After inspection of the resulted forces clearly unphysical values were discarded.

3. Results and discussion

3.1. Pull-off forces on rough surfaces

The measured forces resulted in rather broad distributions as shown in Fig. 3 for one of the tips on the two smoothest surfaces. Although broad scatter of forces is evident, the distributions have clear maxima. The potential creep effects due to repeated measurements over several lateral locations are small enough to fall within the scatter of the data. Since the nature of the measured force distributions was highly asymmetric, mode values for each set were used as the representative force. Due to the same reason inaccuracy estimates were calculated for both sides separately.

Pull-off forces on all three surfaces are shown in Fig. 4. For 10 and 130 nm coatings, linear dependence of the pull-off force on the particle area is clearly seen. For 500 nm surface, the force

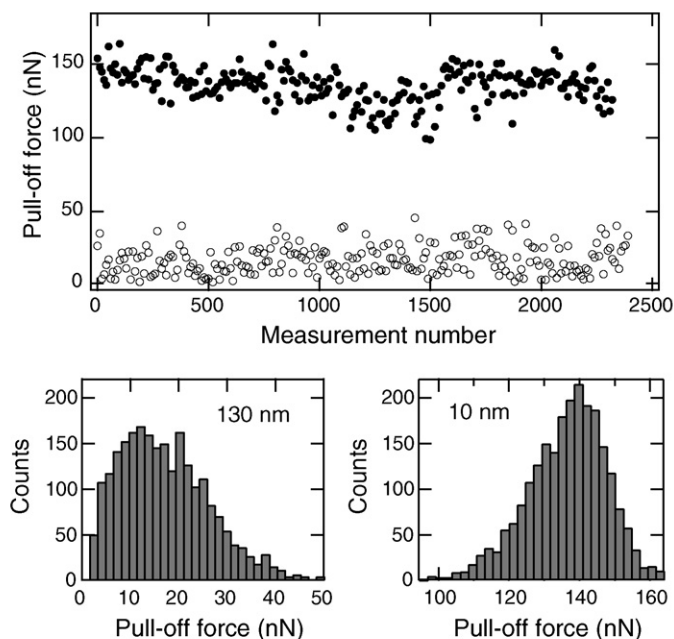

Fig. 3. Pull-off forces and resulting force histograms measured with one of the tips on 10 nm coating (●) and 130 nm coating (○). For clarity, only every tenth force is shown in the upper picture.

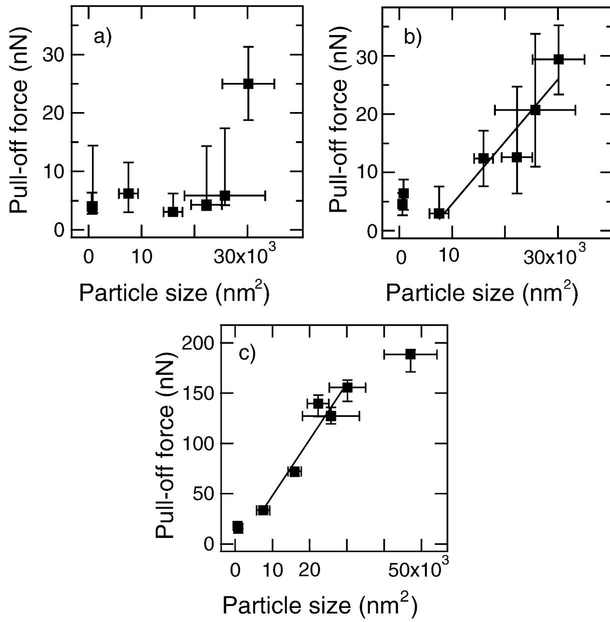

Fig. 4. Pull-off forces measured from rough surfaces as a function of particle size. (a) 500-, (b) 130-, and (c) 10-nm thick coating. The solid lines guide the eye only.

is independent of the particle size except for the largest particle. The scatter in the measured forces increases significantly with with surface roughness.

3.2. Proposed model

The Rabinovich model was derived for spherical particles adhering on rough surface. Since we measured adhesion of blunt particles, we modified the model shown in Eq. (1) to be suitable for blunt particles, or smooth surface, adhering to rough surfaces. We used the same assumptions as used in deriving Eq. (1) in Ref. [7], i.e., contact interaction with one asperity and noncontact interaction with the substrate. The geometry is shown in Fig. 5b. The contact part now comes from the contact between the asperity and the flat particle and the noncontact interaction from the two parallel plates of area A. Equation (1) may be rewritten for the new geometry as

$$F_{adh} = \frac{\mathcal{A}_H}{6H_0^2}\left[r + \frac{A}{\pi H_0(1 + y_{max}/H_0)^3}\right], \tag{3}$$

where the first part is the interaction of the adhering particle with an asperity of radius r and the second part is the interaction with the substrate. In order to avoid significant double counting of the substrate Eq. (3) is valid if the area of the adhering particle is much larger than the area of the asperity, i.e.,

$$A \gg r^2. \tag{4}$$

When the measured pull-off forces are compared to forces predicted by Eq. (3), the model clearly underestimates the adhesion with large particles. This is because the model assumes only one asperity in contact with the particle which obviously fails for large blunt particles. For particles which are of similar size or smaller than the surface features, the model gives reasonable estimates.

In order to predict adhesion on surfaces containing features much smaller than the particles, a model which takes multiple contacts into account is needed. Number of possible contact points for flat particles may be calculated as the average number of asperities under the particle $N = A\rho$ as illustrated in Fig. 5c. Multiplying the contact interaction part in Eq. (3) by N results in

$$F_{adh} = \frac{\mathcal{A}_H A}{6H_0^2}\left[\rho r + \frac{1}{\pi H_0(1 + y_{max}/H_0)^3}\right]. \tag{5}$$

Again, the first part corresponds to the interaction of the adhering particle with the asperities and the second the interaction with the substrate. If the asperities are too densely packed compared to their radius of curvature, multiple counting takes place. This leads to restriction

$$\rho \ll 1/r^2, \tag{6}$$

which also ensures that the error produced by counting noncontact interaction twice under the asperities is negligible if the adhering particle is large. For small particles also (4) have to be considered. These restrictions indicate that (5) cannot be used for surfaces with densely spaced low asperities, resulting in large r and high ρ.

The model in Eqs. (1), (3), and (5) ignores all chemical interactions in the contact areas, leaving only the van der Waals interaction. To estimate the contribution due to the chemical interactions, atomistic simulations using two hydrogenated silica surfaces were made. The increase in the adhesion force was 40–50% of van der Waals force for a flat contact (O.H. Pakarinen, A.S. Foster, Helsinki University of Technology, private communication). The estimates of the chemical interaction agree with previous molecular dynamics simulations [18]. This increase was effectively included into Eq. (5) by slightly reducing the equilibrium distance parameter H_0 from the value obtained from the atomistic simulations. Although we do not explicitly know the nature of the contact area in atomic detail, we believe this approach gives a reasonable approximation of the chemical

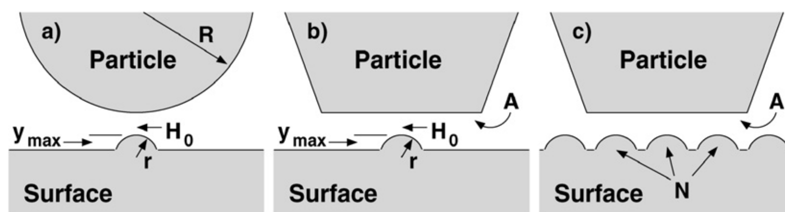

Fig. 5. Contact geometries in different approaches (a) Eq. (1), (b) Eq. (3), and (c) Eq. (5).

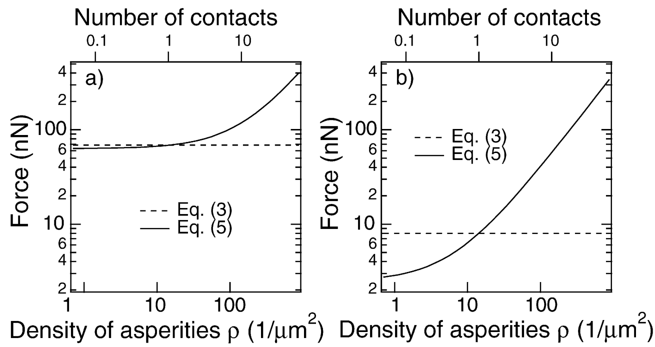

Fig. 6. Comparison of Eqs. (3) and (5) with two different asperity heigths (a) $y_{max} = 1.5$ and (b) 5 nm. Other parameters used: $\mathcal{A}_H = 99.1$ zJ [19], $H_0 = 3$ Å, $A = 70{,}000$ nm^2, and $r = 30$ nm.

interactions present. The experimental estimates [18], and references therein, which show significant contribution from the OH interactions are for extremely flat silica samples. Our measured contacts are not flat and the bonding happens only on small percentage of the total vdW-interaction area, reducing its significance to the total interaction.

Fig. 6 compares Eqs. (3) and (5). There is no dependency on the density of asperities in Eq. (3) but the new Eq. (5) gives increasing forces when the density of asperities is increased. This results in much higher pull-off forces when the density of asperities is high compared to the size if the probe. If the asperities on the surface are low as in Fig. 6a the noncontact interaction is dominating with low asperity densities and Eq. (5) gives reasonable estimates over the whole range. With higher asperities, as in Fig. 6b, the contribution of the noncontact part is negligible and Eq. (5) gives unphysical values with low asperity densities. In this region Eq. (3) should be used.

Fig. 7 shows the agreement between the measured pull-off forces and values predicted by Eq. (5). The contribution of the noncontact interaction is negligible for these asperity heights and it could be omitted.

Fig. 8 combines measured forces from all three TiO_2 surfaces in one plot as a function of number of possible contacts N.

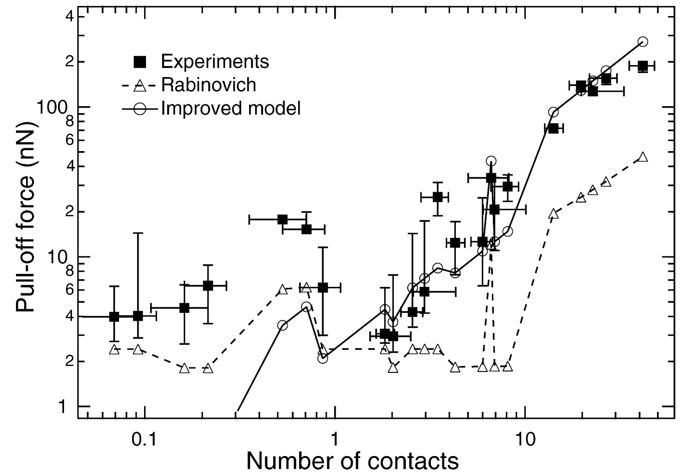

Fig. 8. All experimental values collected and compared to our combined model using Eqs. (3) and (5). The lines are to guide the eye only. Both models are needed to cover the whole range of data.

Also values calculated using models (3) and (5) are included. The calculated values do not form smooth curves since the values depend on the experimentally determined curvature of the asperities on the surface. The values $N < 1$ in Fig. 8 mean that the particle in contact is smaller than the average area covered by one asperity. Since only the apex of the asperity contributes to the interaction, N should equal one even for particles much smaller than the asperities. Eq. (5) leads to unphysical values in this area. Combining Eq. (3), for $N \leqslant 1$ and (5), for $N > 1$, gives excellent agreement with the experimental data measured over three orders of magnitude in the particle/asperity length scales.

4. Conclusion

The strength of the adhesion of small particles on rough surfaces is mainly determined by the geometrical effects of the surface–particle system. The adhesion of particles smaller or similar in size than the dominant surface features is only weakly

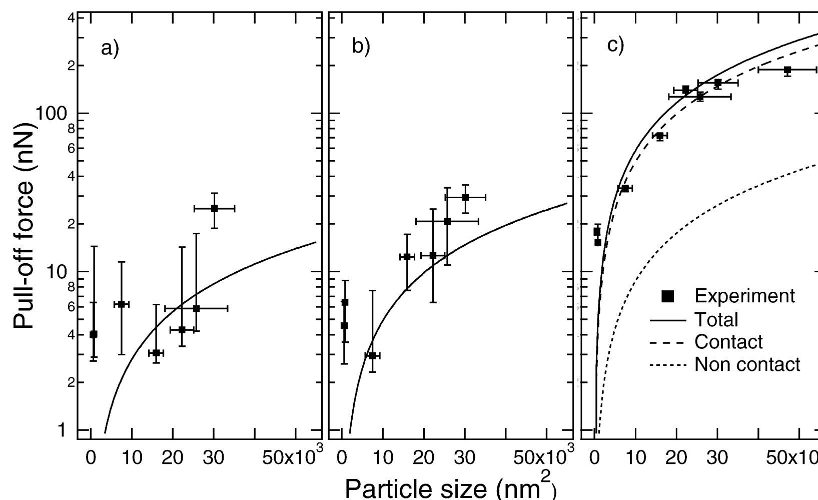

Fig. 7. Comparison of measured forces to estimated values from Eq. (5). (a) 500-, (b) 130-, and (c) 10-nm thick coating. $\mathcal{A}_H = 99.1$ zJ [19], $H_0 = 3$ Å, r and y_{max} from Table 1. The noncontact part is not visible in (a) and (b) since it is less than 0.1 nN.

dependent on the particle size. The interaction is limited to one contact between the particle and a single asperity and the strength of the adhesion is determined by this contact alone. Particles much larger than the surfaces features have several contacts with the surface leading to interaction where, in addition to the asperity geometry, the size of the particle has a major influence on the adhesion. In this study we have shown that the relative size of the adhering particle and the surface features play the most important role in the interaction. We have developed the new model for estimating adhesion that takes this size dependence into account. Comparison of the model to experimental data shows good agreement over a wide range of data.

Acknowledgment

The authors thank Dr. Unto Tapper and Professor Esko Kauppinen at VTT for SEM images and the Finnish Funding Agency for Technology and Innovation (TEKES) for financial support via PINTA Research Program.

References

[1] Y. Samitsu, Nanotechnology 4 (1993) 236.
[2] H. Krupp, Adv. Colloid Interface Sci. 1 (1967) 111.
[3] D. Tabor, J. Colloid Interface Sci. 58 (1977) 2.
[4] B.J. Briscoe, S.S. Panesar, J. Phys. D Appl. Phys. 25 (1992) A20.
[5] H.-J. Butt, B. Cappella, M. Kappl, Surf. Sci. Rep. 59 (2005) 1.
[6] H. Rumpf, Particle Technology, Chapman & Hall, London/New York, 1990.
[7] Y.I. Rabinovich, J.J. Adler, A. Ata, R.K. Singh, B.M. Moudgil, J. Colloid Interface Sci. 232 (2000) 10.
[8] Y.I. Rabinovich, J.J. Adler, A. Ata, R.K. Singh, B.M. Moudgil, J. Colloid Interface Sci. 232 (2000) 17.
[9] K. Cooper, N. Ohler, A. Gupta, S. Beaudoin, J. Colloid Interface Sci. 222 (2000) 63.
[10] K. Cooper, A. Gupta, S. Beaudoin, J. Colloid Interface Sci. 234 (2001) 284.
[11] M. Götzinger, W. Peukert, Vacuum 20 (2004) 5298.
[12] S. Eichenlaub, A. Gelb, S. Beaudoin, J. Colloid Interface Sci. 280 (2004) 289.
[13] E.R. Beach, G.W. Tormoen, J. Drelich, R. Han, J. Colloid Interface Sci. 247 (2002) 84.
[14] G.W. Tormoen, J. Drelich, J. Nalaskowski, J. Adhesion Sci. Technol. 19 (2005) 215.
[15] M. Leskelä, M. Ritala, Thin Solid Films 409 (2002) 138.
[16] V. Pore, A. Rahtu, M. Leskelä, M. Ritala, T. Sajavaara, J. Keinonen, Chem. Vap. Deposit. 10 (2004) 143.
[17] J.E. Sader, J.W.M. Chon, P. Mulvaney, Rev. Sci. Instrum. 70 (1999) 3967.
[18] D.A. Litton, S.H. Garofalini, J. Appl. Phys. 89 (2001) 6013.
[19] R.H. French, R.M. Cannon, L.K. DeNoyer, Y.-M. Chiang, Sol. St. Ionics 75 (1995) 13.